Series Editor
André Mariotti

Paleobiology of Giant Flightless Birds

Delphine Angst
Eric Buffetaut

Color section

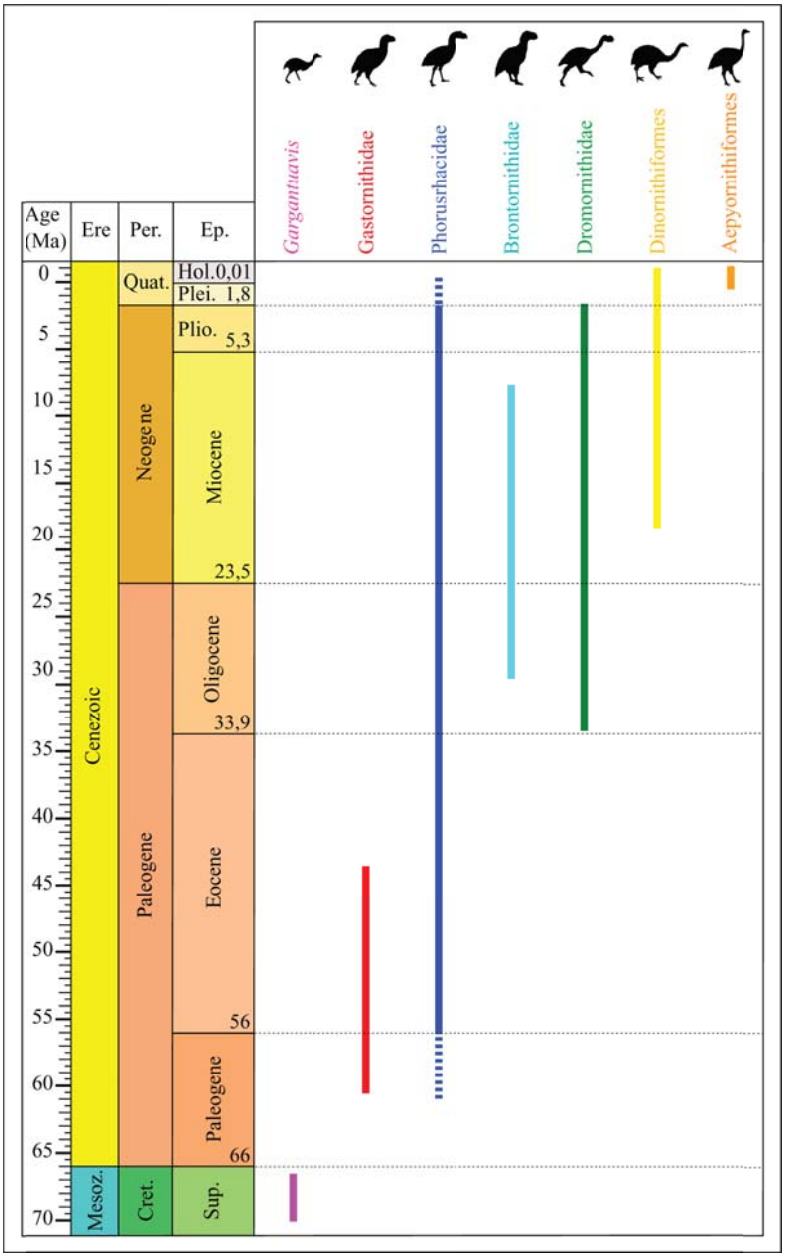

Figure 1.1. *Stratigraphic distribution of the large fossil and subfossil terrestrial birds*

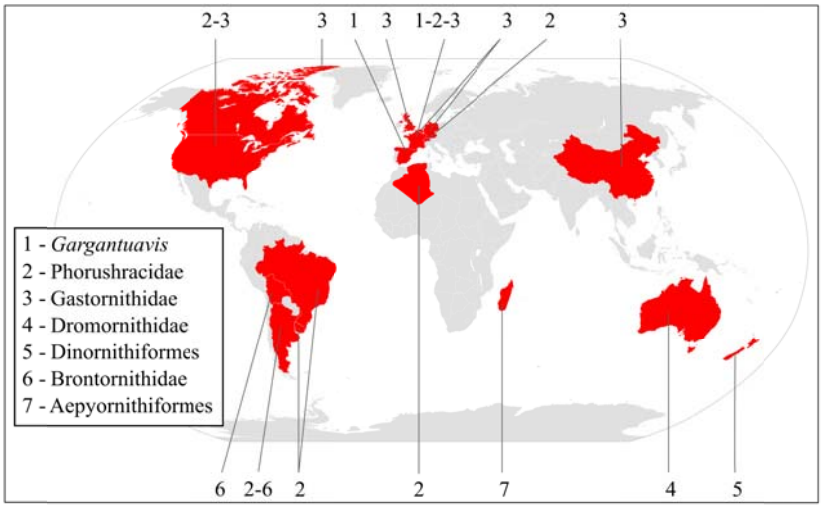

Figure 1.2. *Geographical distribution of large fossil and subfossil birds mentioned in text*

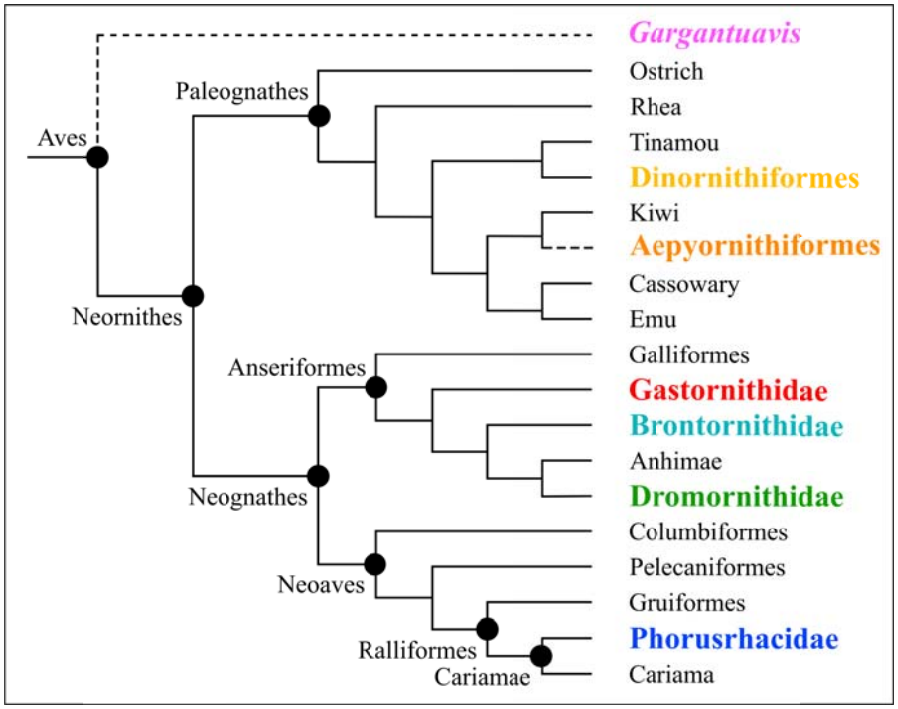

Figure 1.3. *Simplified phylogeny of the large fossil and subfossil terrestrial birds*

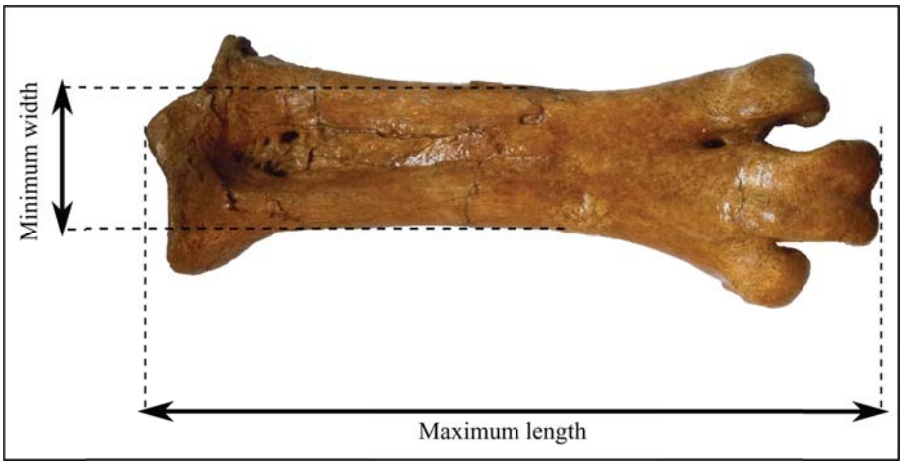

Figure 1.5. *Location of the measurements on the tarsometatarsus according to Angst* et al. *(2016)*

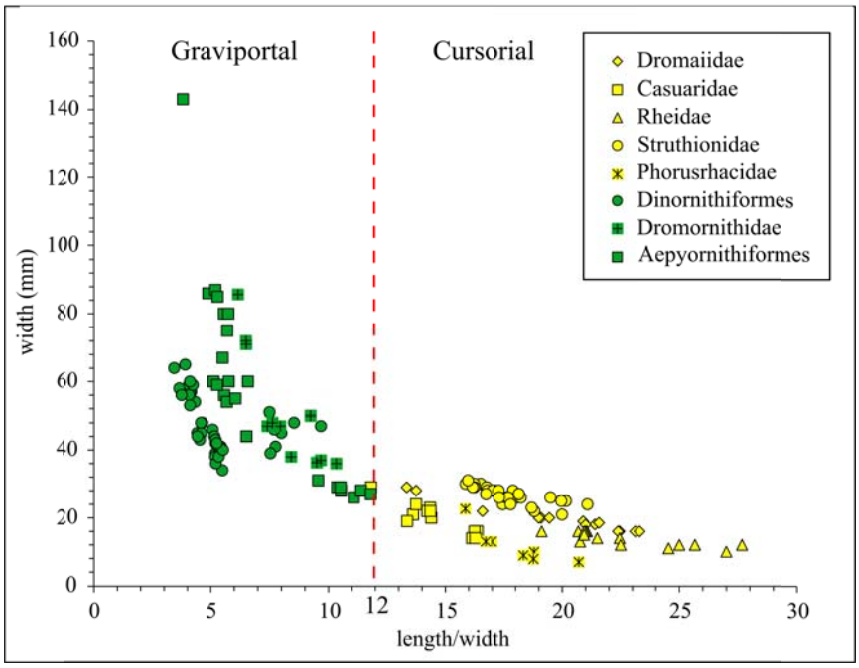

Figure 1.6. *Estimation of the locomotion type through the method of Angst* et al. *(2016)*

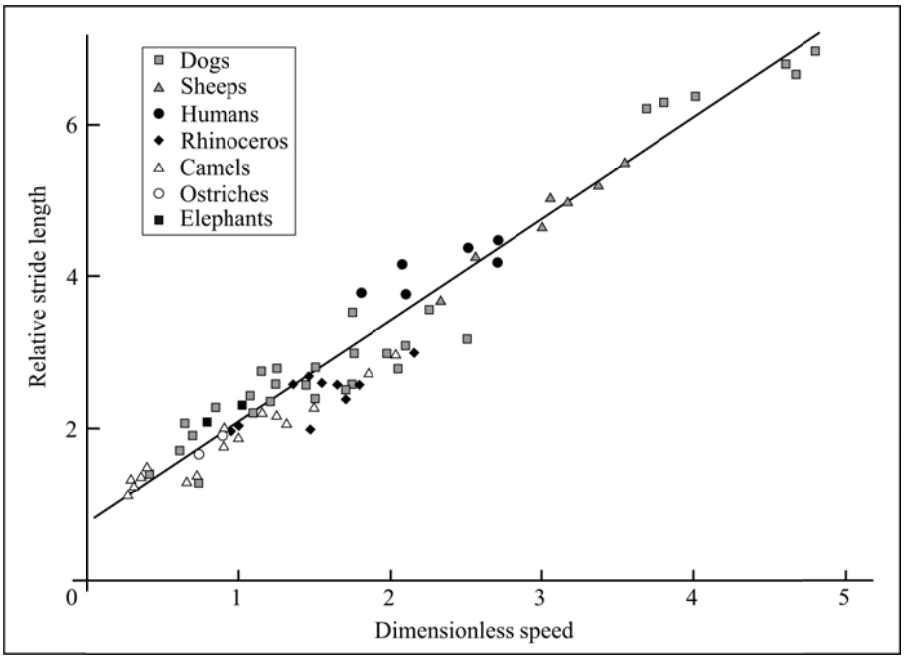

Figure 1.7. *Graph of dimensionless speed according to the relative stride length for various terrestrial vertebrates. From Alexander (1989)*

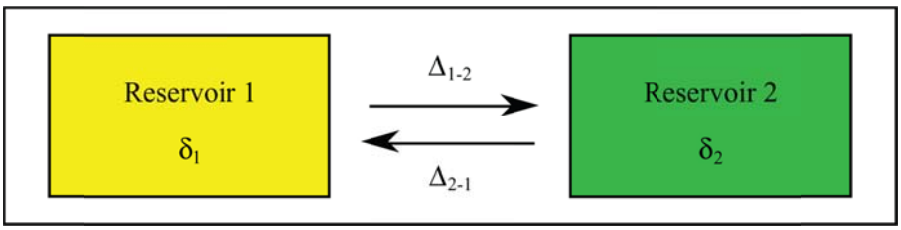

Figure 1.11. *Diagram illustrating the isotope fractionation between two reservoirs*

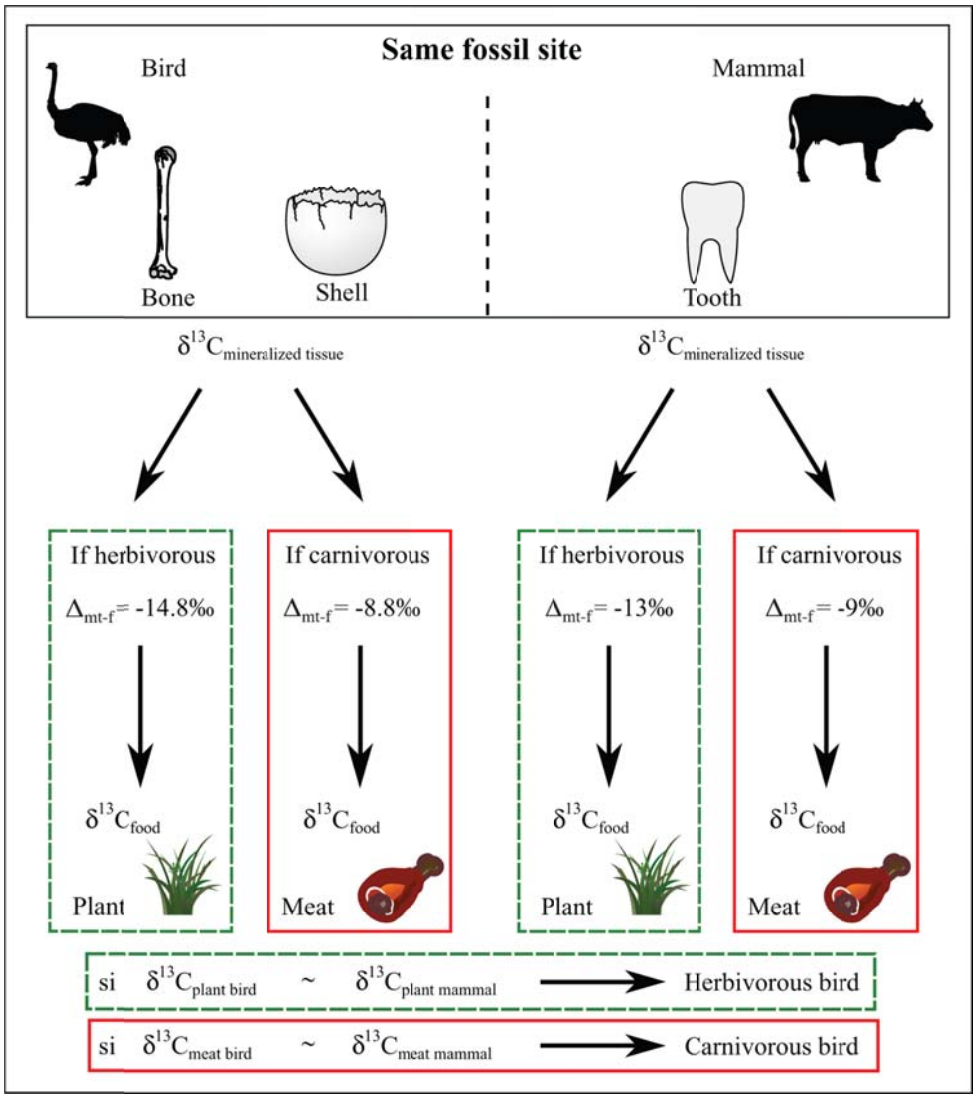

Figure 1.12. *Diagram of the estimation of a bird diet from the $\delta^{13}C$ of its mineralized tissues (mt) (eggshell or bone) compared with the mineralized tissues of mammals (tooth) from the same fossil site*

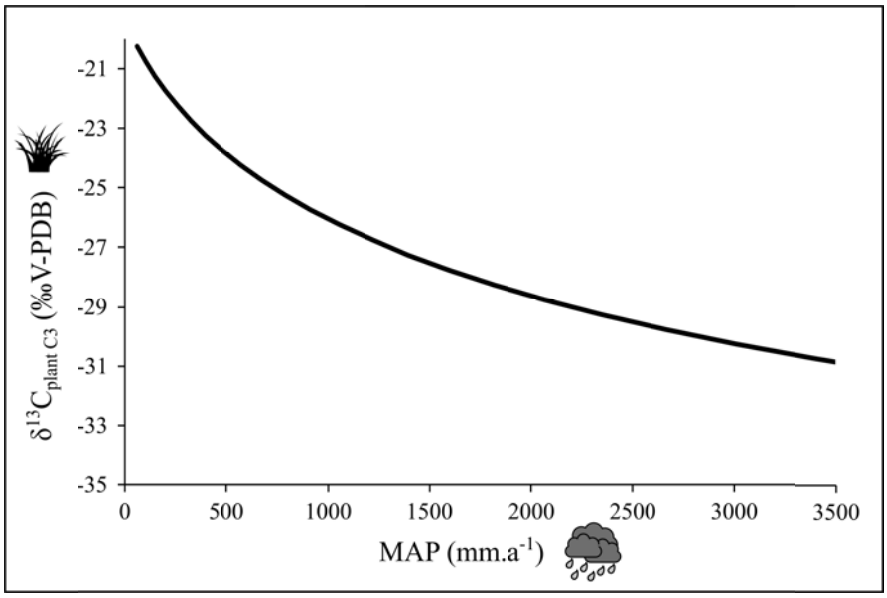

Figure 1.14. *Graph of the $\delta^{13}C$ of the C3 plants as a function of the mean annual precipitations (MAP) according to the equation formulated by Rey* et al. *(2013)*

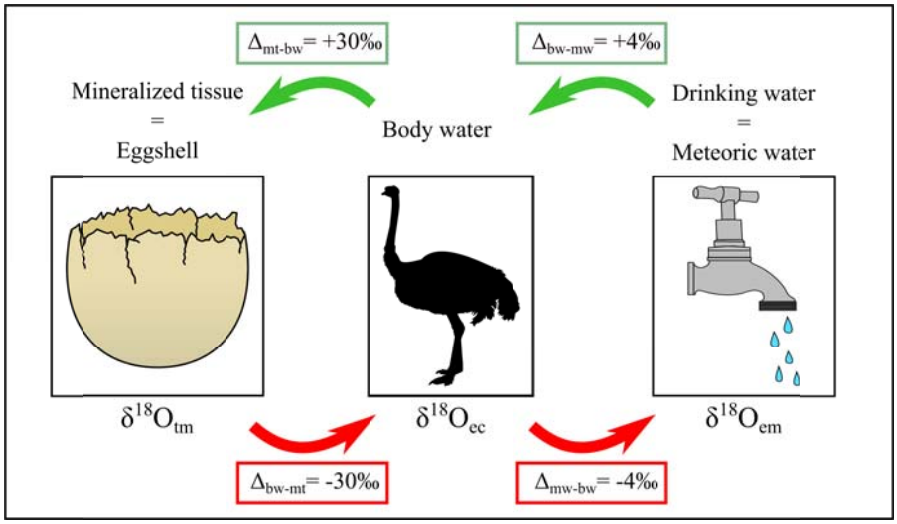

Figure 1.15. *Diagram of the different estimation stages of the $\delta^{18}O$ of meteoric water from the $\delta^{18}O$ of eggshells. mt: mineralized tissue; bw: body water; mw: meteoric water; green arrows: isotope fractionation values established from extant ostriches; red arrows: isotope fractionation values to be used to estimate the $\delta^{18}O$ of meteoric water from the $\delta^{18}O$ of fossil eggshells*

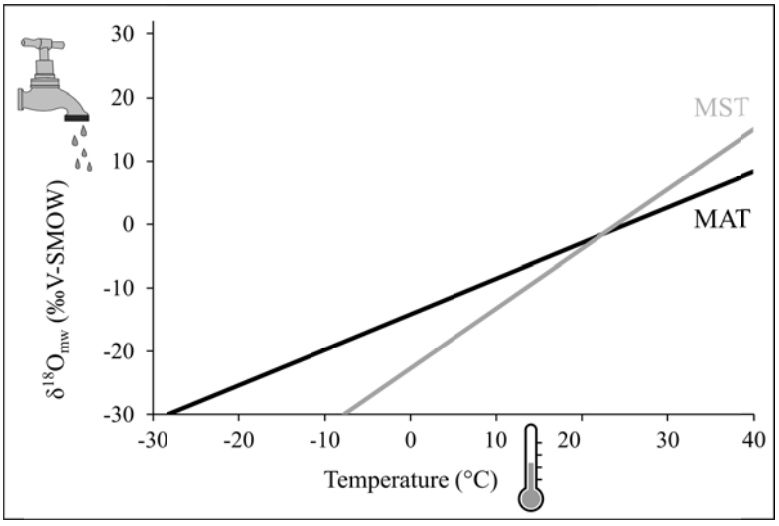

Figure 1.16. *Graph of the $\delta^{18}O$ meteoric water (mw) compared with the mean annual temperature (MAT, black line) according to Lécuyer (2013), or compared with the mean summer temperature (MST, gray line) according to Bernard* et al.. *(2009)*

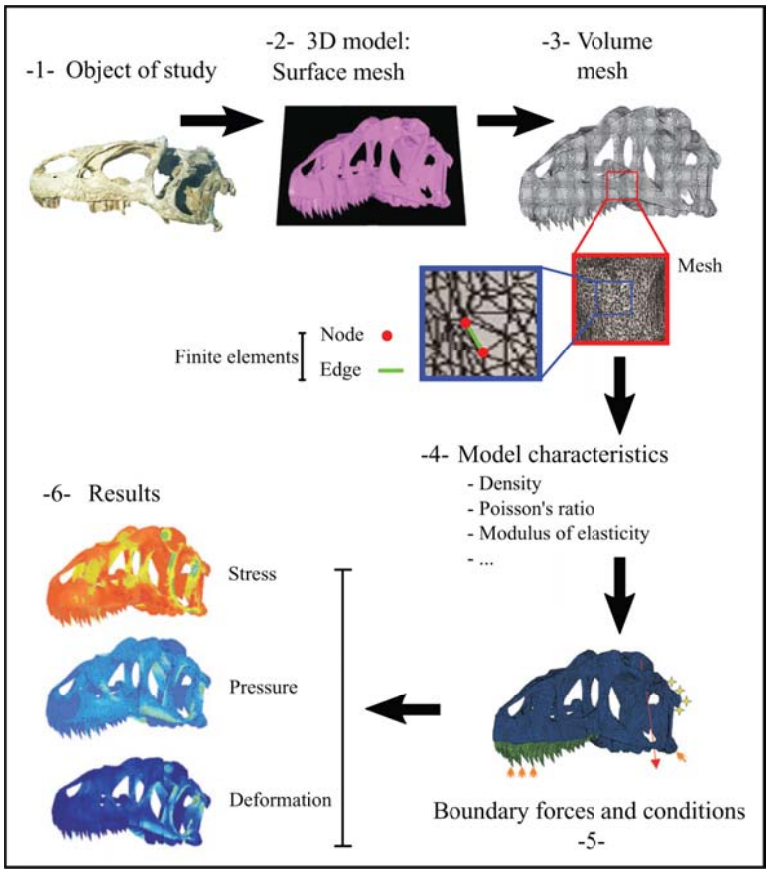

Figure 1.18. *Successive stages of the finite element analysis (after Rayfield, 2007)*

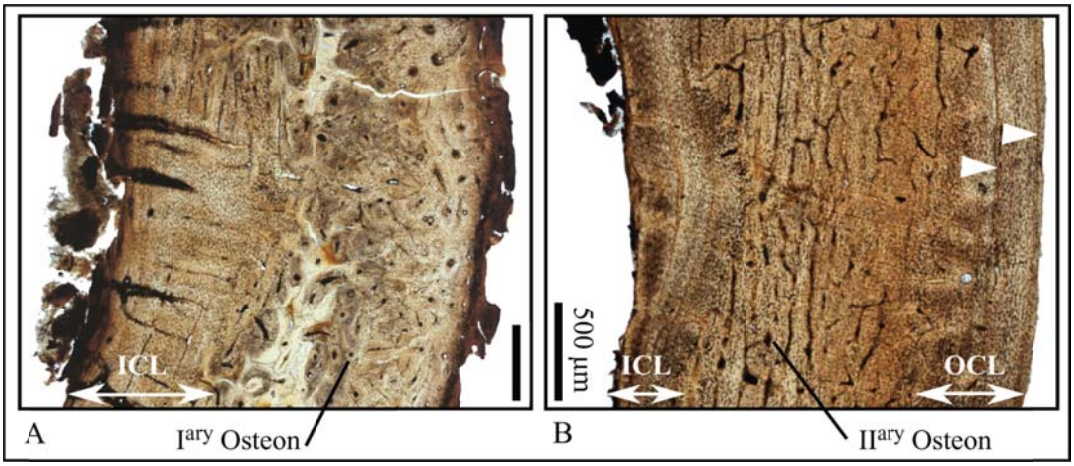

Figure 1.20. *Photograph of thin sections of* Raphus cucullatus*. A – Tibiotarsus of a juvenile. B – Femur of an adult showing lines of arrested growth in the OCL. ICL: inner circumferential layer; OCL: outer circumferential layer; white arrows: lines of arrested growth (LAGs); I^{ary} osteon: primary osteon; II^{ary} osteon: secondary osteon (from Angst* et al*. 2017)*

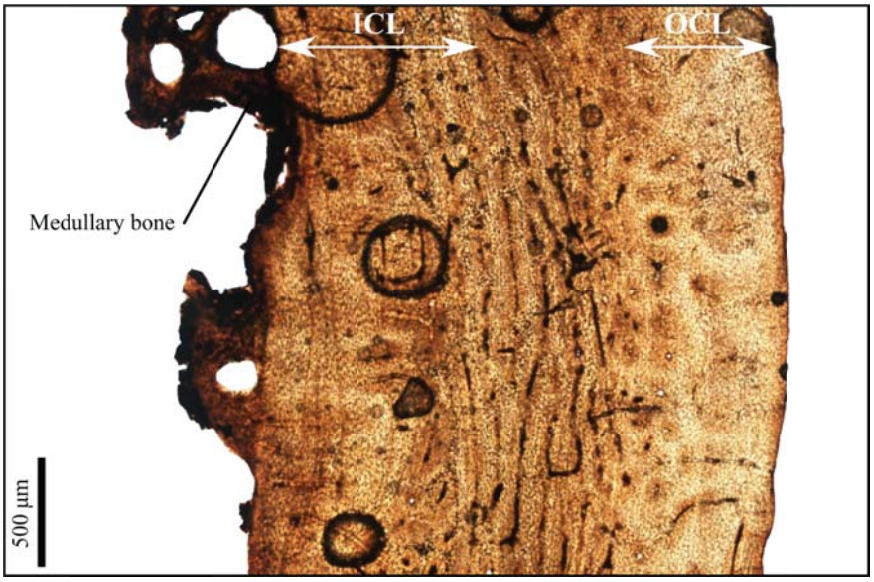

Figure 1.21. *Photograph of a thin section of a* Raphus cucullatus *femur with medullary bone indicating that it is an ovulating female (from Angst* et al*. 2017)*

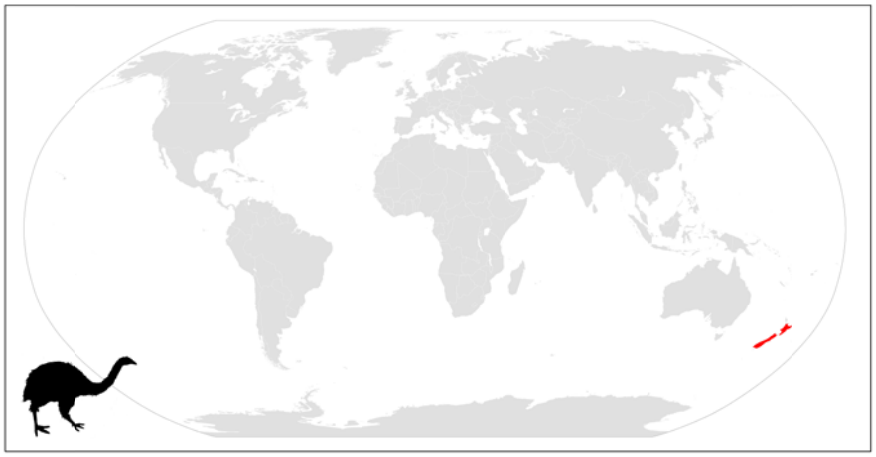

Figure 2.2. *Geographical distribution of Dinornithiformes*

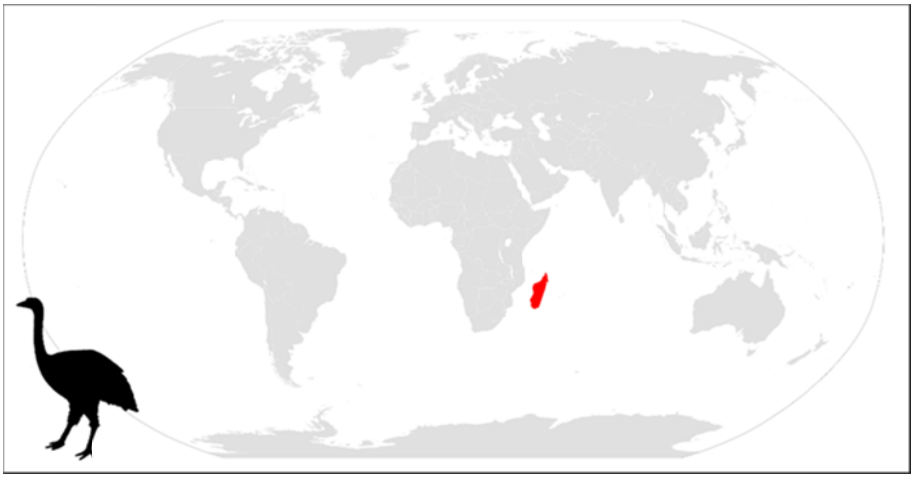

Figure 3.2. *Global geographic distribution of Aepyornithiformes*

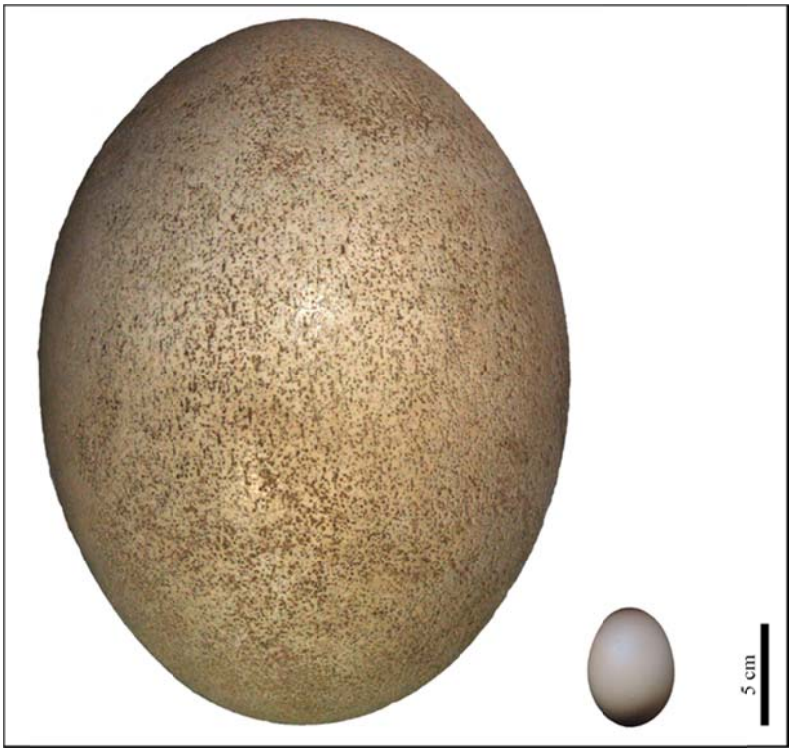

Figure 3.8. *Eggs of* Aepyornis *(on the left, photo E. Buffetaut) compared with a hen's egg (on the right, photo D. Angst)*

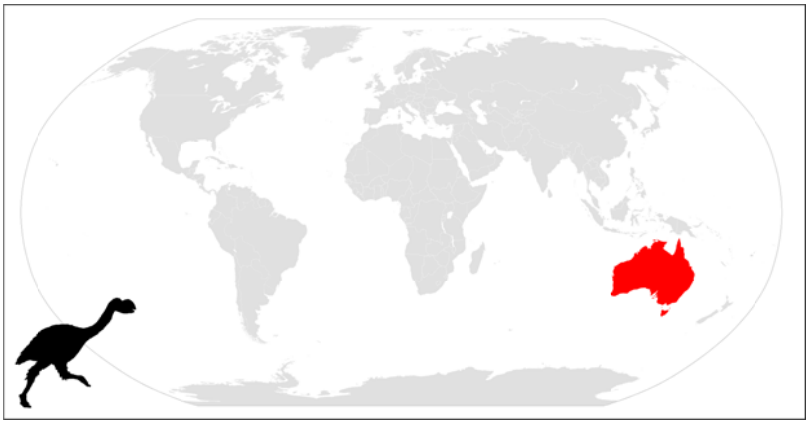

Figure 4.2. *Global geographical distribution of Dromornithidae*

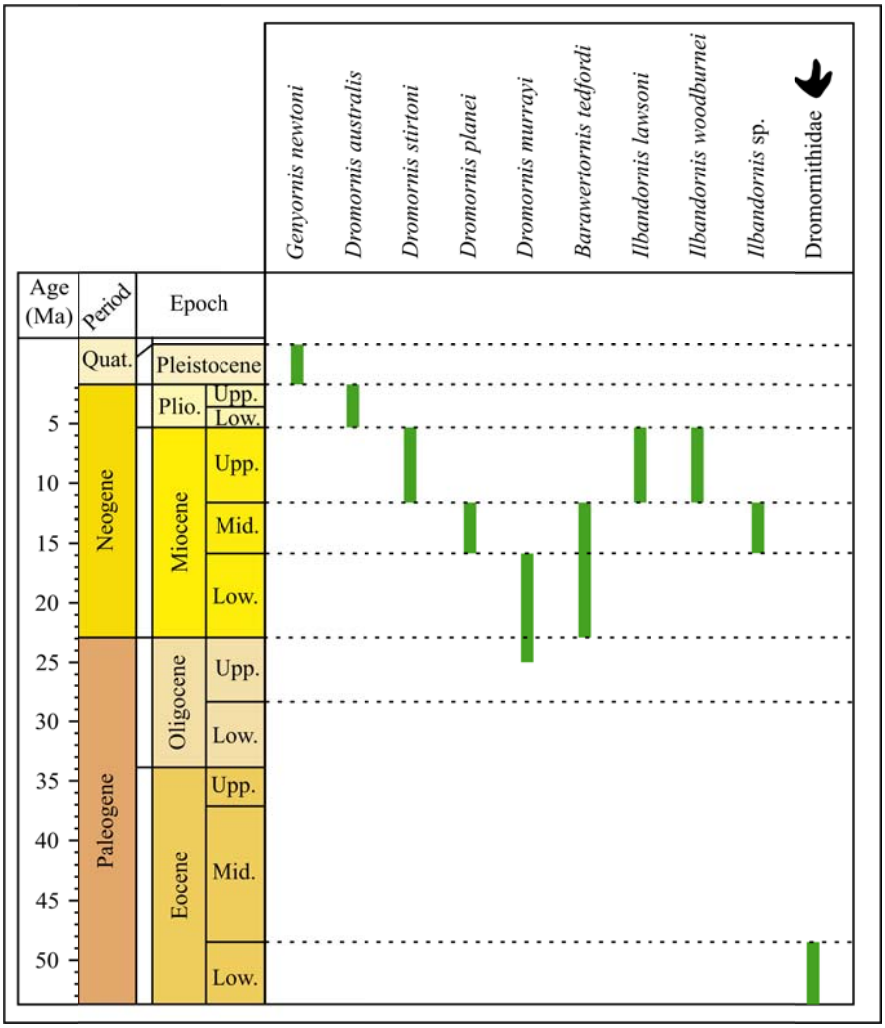

Figure 4.3. *Simplified stratigraphic distribution of Dromornithidae.* : *footprints*

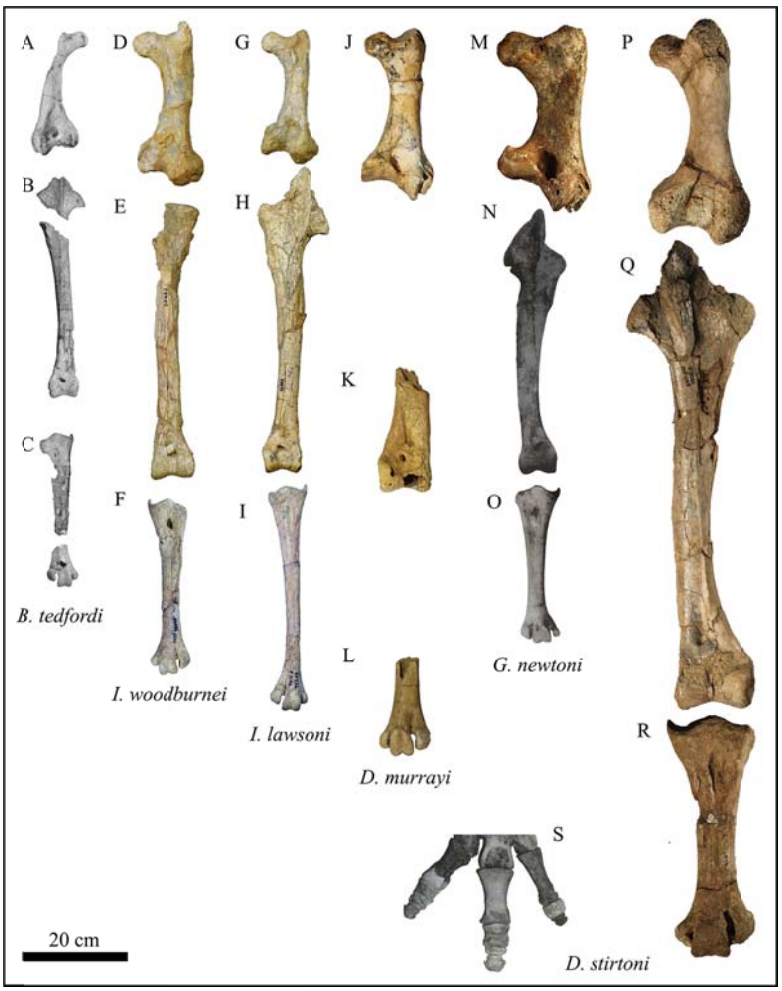

Figure 4.7. *Bones of the hindlimbs of some Dromornithidae. A, D, G, J, M, N: femurs; B, E, H, K, N, Q: tibiotarsi; C, F, I, L, O, R: tarsometatarsi; Q: phalanges. Images A-C from Nguyen* et al. *(2010), images D-I from Worthy & Yates (2015), images J-L from Worthy* et al. *(2016) image M from Grellet-Tinner* et al. *(2016), images P-R from Handley* et al. *(2016) and images, N, O, Q drawn by Murray & Vickers-Rich (2004);* B. tedfordi*:* Barawertornis tedfordi, I. woodburneyi*:* Ilbandornis woodburneyi, I. lawsoni*:* Ilbandornis lawsoni, D. murrayi*:* Dromornis murrayi, G. newtoni*:* Genyornis newtoni, D. stirtoni*:* Dromornis stirtoni

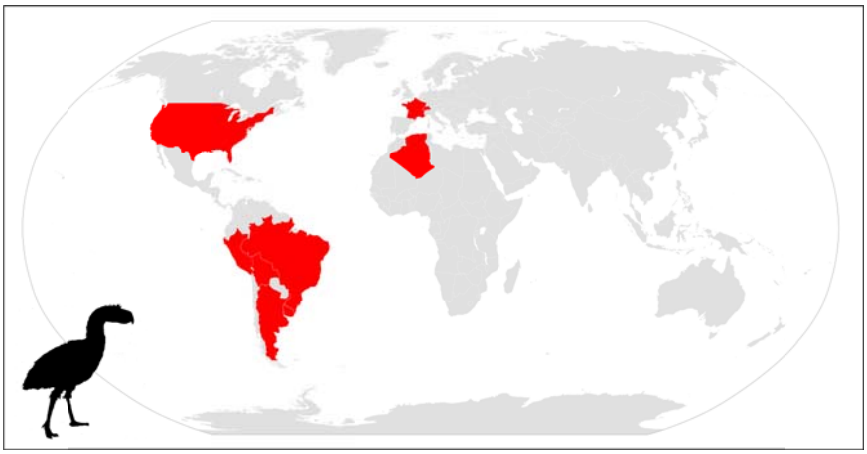

Figure 5.2. *Geographical distribution of the countries where body fossils of Phorusrhacidae have been discovered*

Figure 5.8. *Cast of the skull (A) and mandible (B) of* Andalgalornis steulleti *(specimen n° FM P14357). Photo: Eric Buffetaut*

Figure 5.9. *Pelvis of* Procariama simplex *(MACN 8225) seen dorsally (A) and laterally (B); pelvic limb bones of* Hermosiornis milneedwardsi *(MACN 5944) including a femur (C), a tibiotarsus (D) and a tarsometatarsus (E) (Photos Eric Buffetaut); Tarsometatarsus of* Paraphysornis brasiliensis *(F) (photo Delphine Angst), Tarsometatarsus of* Kelenken guillermoi*, BAR 3877-11 (G) (after Bertelli* et al.*, 2007), terminal phalanges of* Eleutherornis cotei *(H) (after Angst* et al.*, 2013)*

Figure 6.3. *Geographical distribution of the countries where brontornithid remains have been found*

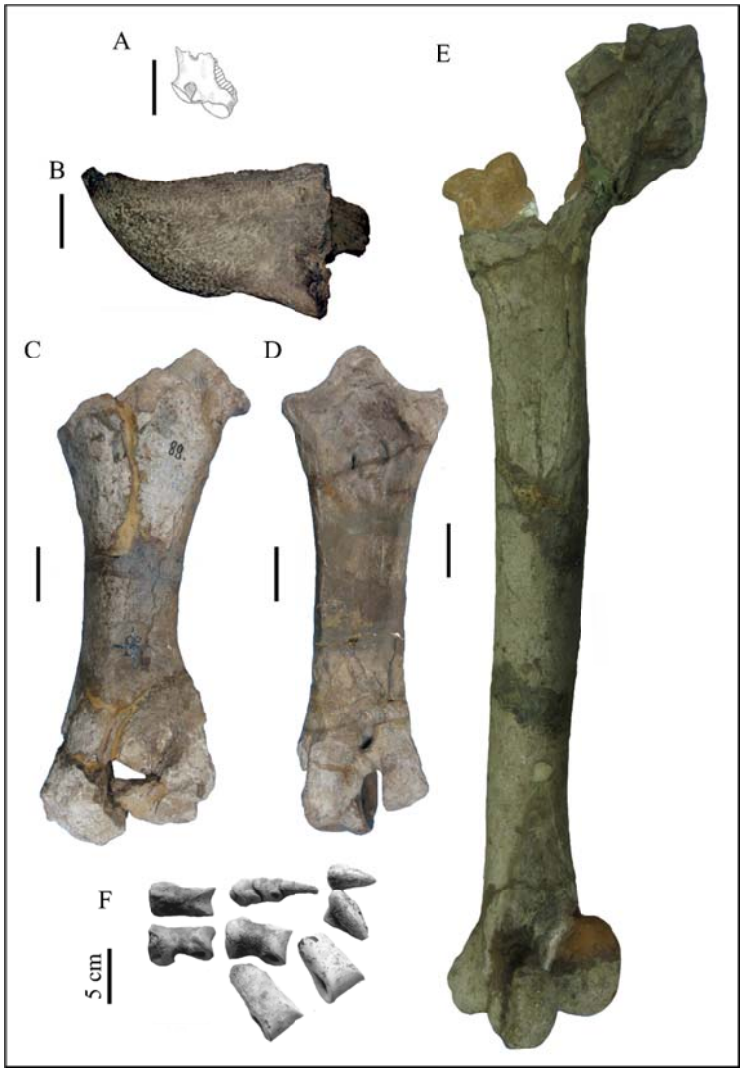

Figure 6.5. *Pictures of the main known bones of* Brontornis. *(A) Quadrate (after Agnolin (2007)), (B) Mandible (according to Agnolin (2007) and Buffetaut (2014), (C) Femur (Photos by Angst and Buffetaut), (D) Tarsometatarsus (Photos by Angst and Buffetaut), (E) Tibiotarsus (Photos by Angst and Buffetaut) and (F) Phalanges (according to Alvarenga & Höfling (2003))*

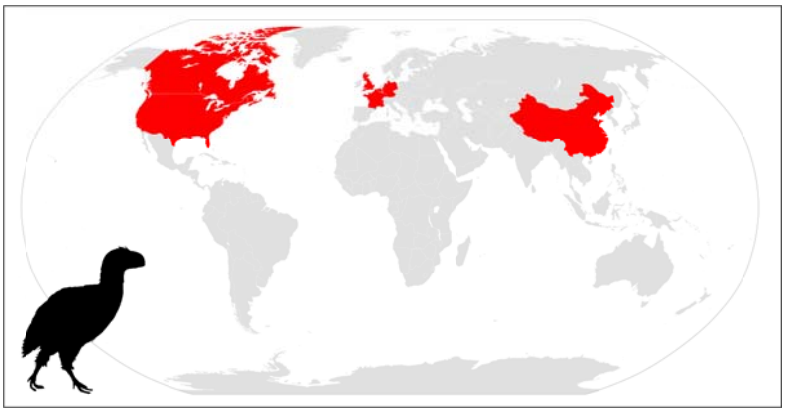

Figure 7.2. *Geographical distribution of the countries where body fossils of Gastornithidae have been found*

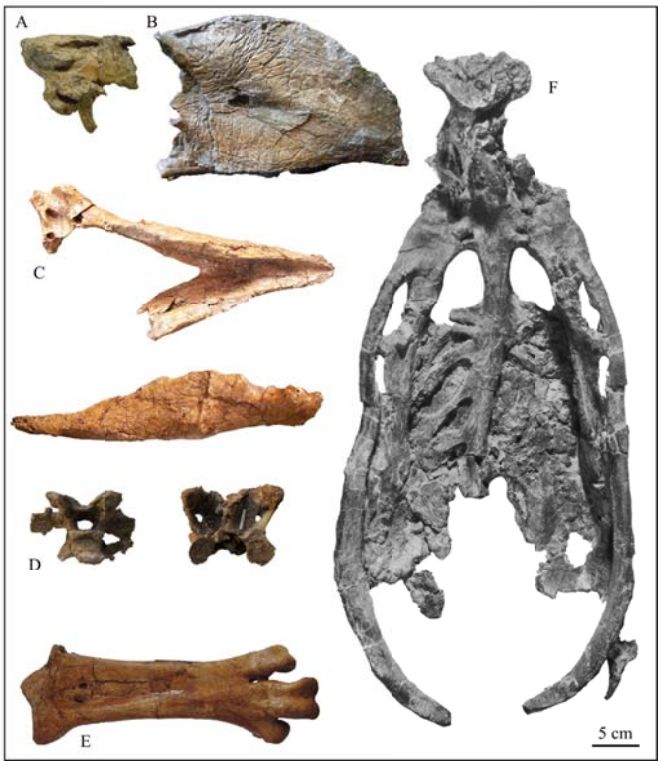

Figure 7.9. *Main skeletal elements of Gastornithidae. (A) Posterior part of skull in lateral view (n° AMNH. 6169), (B) Maxilla in lateral view (n° AMNH. 6169), (C) Mandible in dorsal view (above) and lateral view (below) (n° MHNT. PAL. 1.1.), (D) Vertebrae (left n° MHNT. PAL. 2013.15 in caudal view; right n° MHNT. PAL. 2013.15.6. in dorsal view), (E) Tarsometatarsus in dorsal view (unnumbered, Escuillié collection; cast n° L3092 MNHN), (F) Pelvis in ventral view (n° AMNH. 6169)*

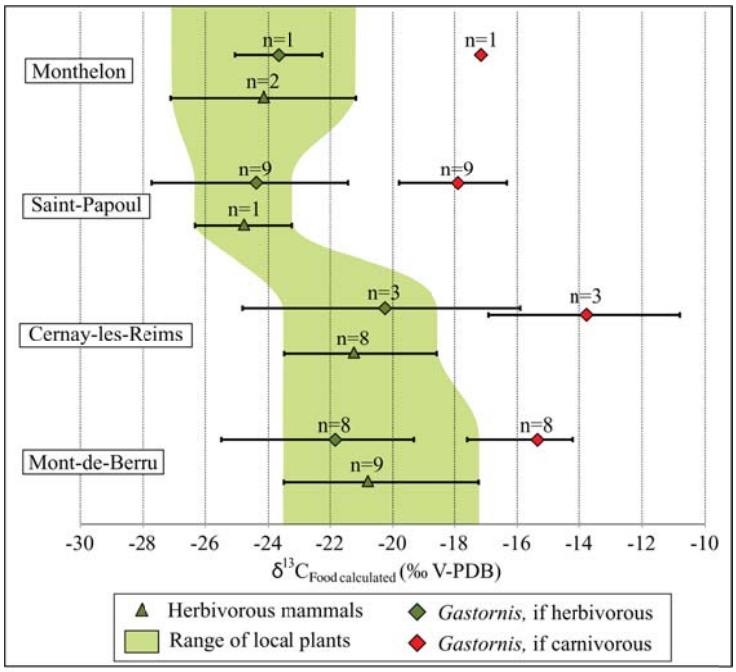

Figure 7.11. *$\delta^{13}C$ of the diet of* Gastornis *and contemporaneous herbivorous mammals from the same fossil sites, estimated from the $\delta^{13}C$ of the apatite of the carbonates for the four sites studied. Range of $\delta^{13}C$ of local plants estimated based on the $\delta^{13}C$ of the fauna of herbivorous mammals from these sites. Horizontal lines: minimum and maximum values, triangle and diamond: mean value, cross-hatched area: boundary between different sites, n: number of specimens. (from Angst* et al.*, 2014a)*

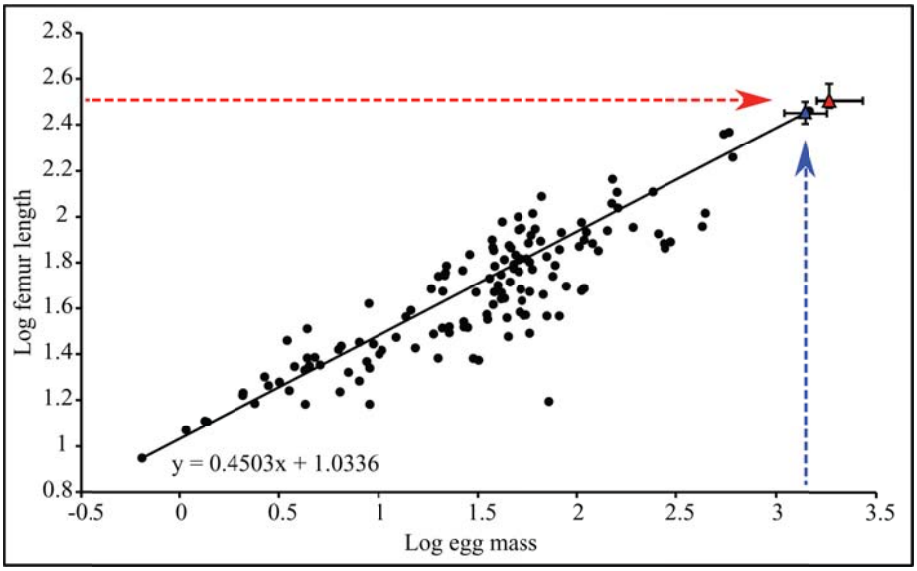

Figure 7.15. *Estimate of the log(femur length) based on the log(egg mass) obtained using the measurements and the regression line published by Dyke and Kaiser (2010) (bottom triangle); compared with the log(egg mass) estimated on the basis of the log(femur length) measured for European* Gastornis *(top triangle). The two values are very similar, suggesting that the fossil eggshells may be attributed to* Gastornis

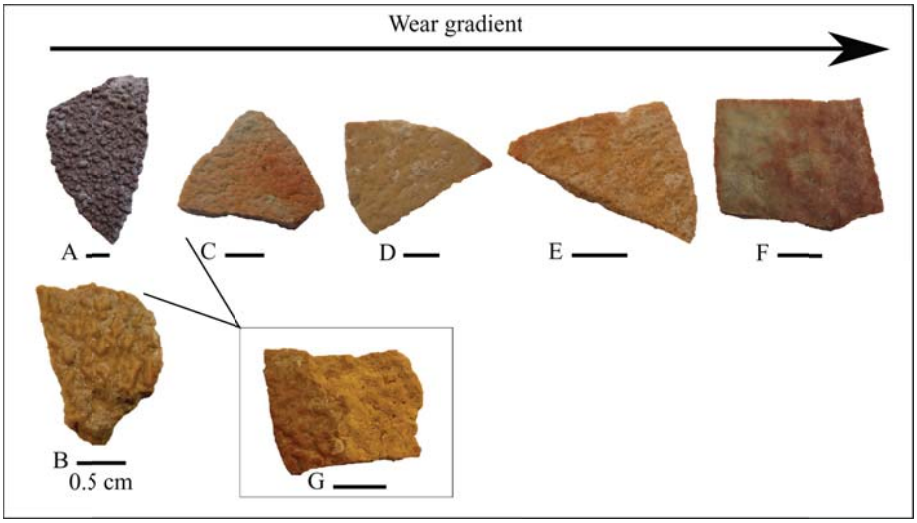

Figure 7.16. *Variation of the external ornamentation on the fossil eggshells of* O. arcuatus *in relation to wear. (A) Mamillated ornamentation, (B) Ornamentation with marked vermiculation, (C) Ornamentation with moderate vermiculation, (D) Ornamentation with fine and spaced-out vermiculation, (E) Semi-smooth ornamentation, (F) Smooth ornamentation, (G) Shells showing the transition between ornamentations B and C*

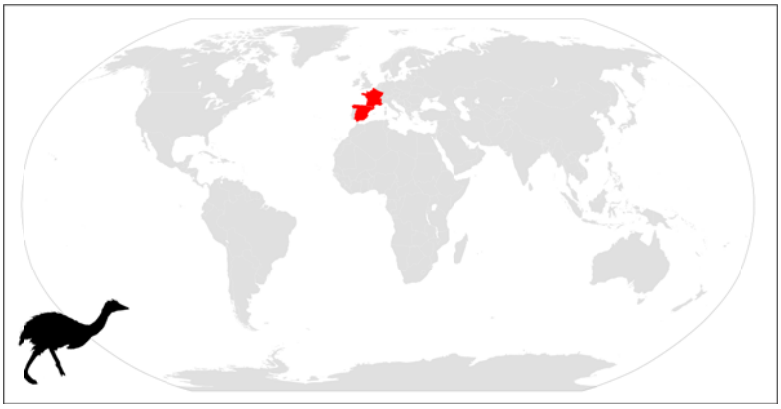

Figure 8.1. *Geographical distribution of* Gargantuavis

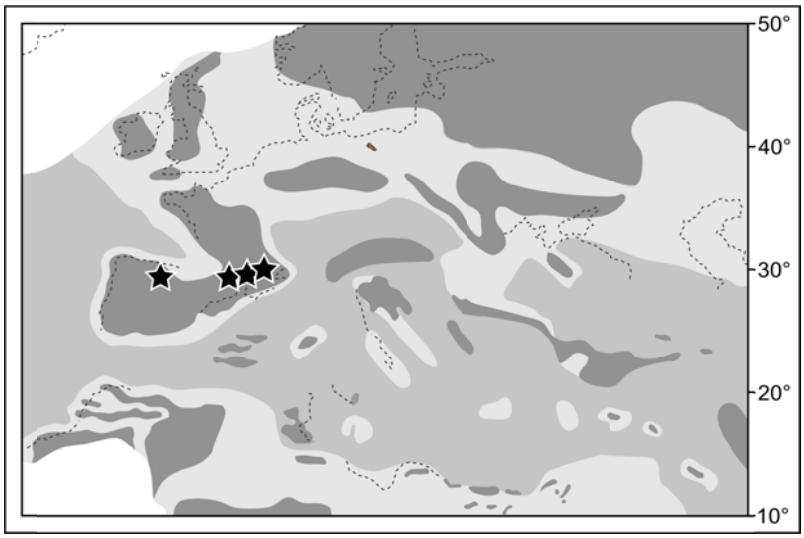

Figure 8.2. *Paleogeographical map of Europe during the Late Cretaceous, showing the distribution of the sites that have yielded* Gargantuavis *(from Buffetaut & Angst, 2016a)*

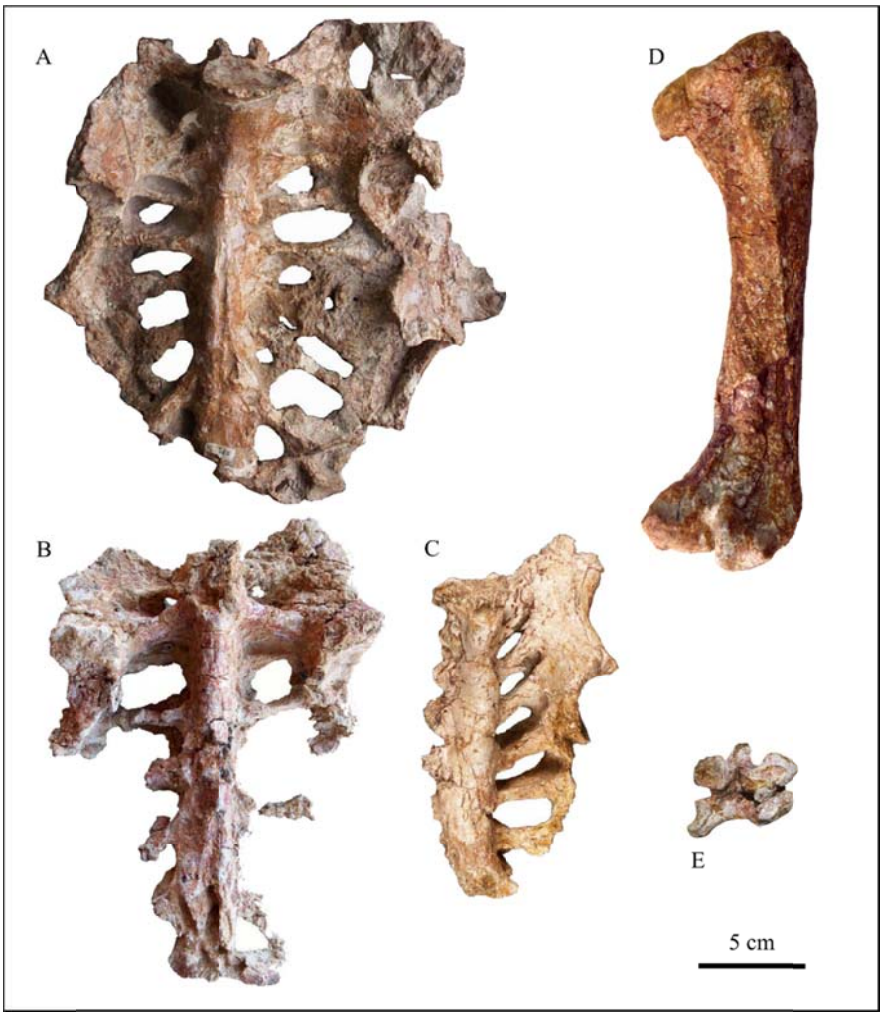

Figure 8.4. *Skeleton elements known to belong to* Gargantuavis philoinos.
(A) Pelvis n° MDE C3-525, (B) Pelvis n° BN 758, (C) Pelvis n° BN 763, (D) Femur n° MN 1335 and (E) Cervical vertebra n° MC-MN476 (photos by Eric Buffetaut)

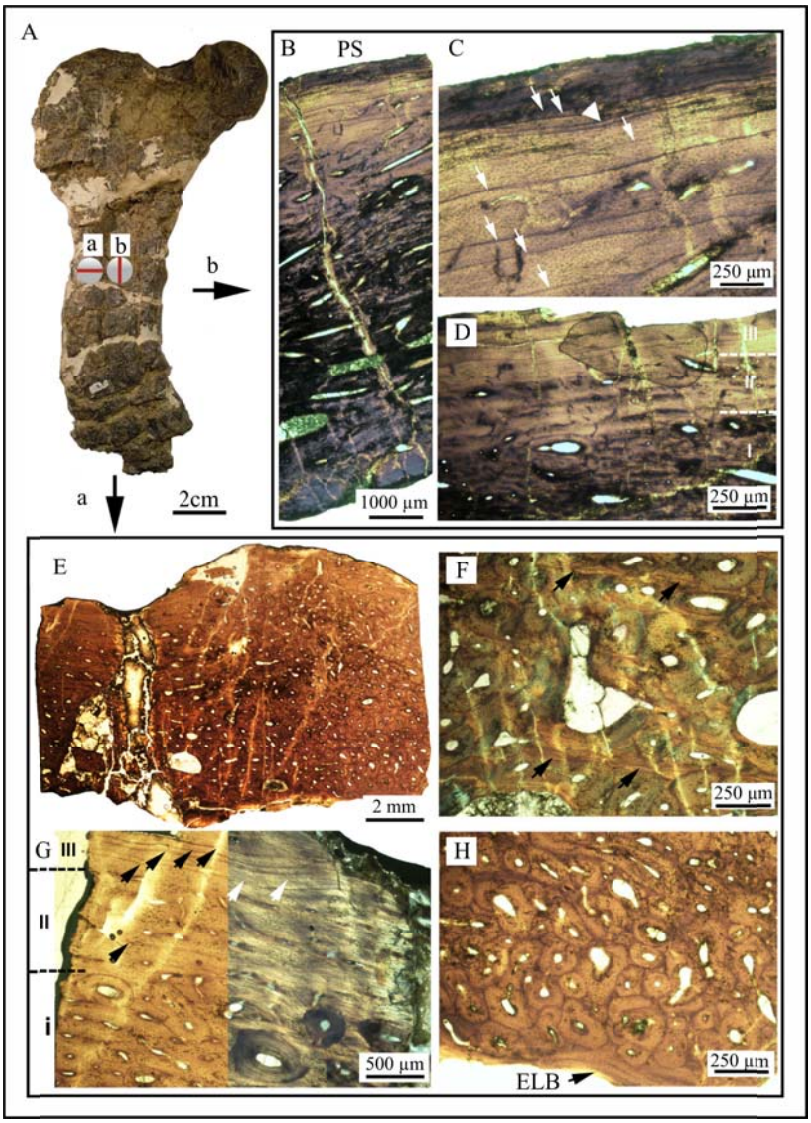

Figure 8.5. *Histology of the femur of* Gargantuavis *(MDE A06). (A) Cranial view of the femur and position of the sites drilled for the histological study, indicated by the gray circles. (B) Part of the longitudinal section of drilling site b. (C) A detail of the outer part of the cortex. (D) A detail of drilling site b showing the change in bone texture. (E) Transversal section of the drilling site. (F, G, H) Details of section a. PS: periosteal surface, ELB: endosteal lamellar bone, White arrows: lines of arrested growth, Thick, white triangle: double line of arrested growth. From Chinsamy* et al. *(2014)*